Summary of noise spectra from Panga GPS network

John Langbein

January 31, 2001

Abstract: The noise characteristics of GPS time series data appear represented adequately by a combination of flicker noise and white noise. For the 21 components from 7 baselines examined, the results shown in Figure 1 indicate that the amplitude of flicker noise is highly correlated with white noise which suggests that the noise detected is due to the combination GPS hardware/software rather than monument noise. If the temporal correlation was monument noise, then I don't believe that the white and colored noise amplitudes would be correlated. At this time, I can not detect confidently any random walk noise due to the monument wobble. Even though random walk noise is not detected in the data, however, the results in Figure 2 show that its presence can still affect the standard errors in rates for intervals greater than 2 months or less assuming that the random walk exceeds $0.5\text{mm}/\sqrt{\text{yr}}$.

The data analyzed here are position changes from 7 sites provided to me by Meghan Miller. The data span between from 2 years at REDM to 7.4 years at ALBH and DRAO. The 7 sites can be grouped into 3 categories. Three sites, CABL, PABH, and REDM, were installed by the PANGA group. These use geodetic quality Trimble receivers and choke ring antennas. At two sites, CABL and PABH, deeply braced monuments were used in marine sediments at these sites along the Pacific Coast. The other site, REDM, is an invar rod grouted into bedrock. All three of these sites should have stable monuments and high quality GPS phase data. However, the record for these sites tend to be short, from 2 to 3 years in length.

The ALBH and DRAO sites are IGS(?) sites using Rogue receivers and choke ring antennas. The monuments consist of 1.5 to 3 meter high cement piers anchored to bedrock. Both sites have data records over 7 years long. ALBH is located on the coast.

The last 2 sites were installed for the Coast Guard. They use high quality Ashtech receivers but non-choke ring antennas (known as a "whopper" antennas). The antennas also are covered by a "snow" dome. Both of these conspire to decrease the quality of the phase data. The site logs do not mention anything about the monuments, but I will assume that these monuments are not as good as the other 5 sites. The record length for these baselines are between 3.5 and 4.5 years.

I evaluated the noise spectra from these sites several ways. First, I used the Maximum Likelihood Estimation (MLE) to find the best fitting data covariance for each time-series. I evaluated 5 different types of noise models and used the MLE technique to adjust the size of the noise components to match the data. (Technique is described by Langbein and Johnson, 1997 *JGR*). The 5 noise models examined are, Random walk, Flicker, Power-law, Random walk plus Band-pass filtered, and Flicker plus Band-pass filtered. All five also include white noise. Random walk and Flicker noise are special cases of Power-law noise with the index set to 2 and 1 respectively. That is, power law noise has a power spectra density of:

$$P(f) = \frac{P_o}{f^n}$$

where n is the index, f is frequency, and P_o is a constant

The other noise component examined is band-pass filter noise. Here, I attempted to model the more complex signal that appears to be seasonal with roughly a 365-day

period. In all cases, I fit and removed a seasonal signal along with the rate when I estimated the noise character of the data. However, the single sine wave doesn't necessarily capture all of the frequencies that might be present in data contaminated with an annual cycle. To capture this complexity, I added an additional covariance term to mimic white noise that had been band-pass filtered with the center frequency of the pass-band at 1-cycle per year. Although I can specify the width of the pass band and the steepness of the curve that defines the pass band, I chose to evaluate only one type of model; a pass band between 0.5 and 1.5 cycles per year with 1-pole.

The results of the improvement of fit for 4 of the noise models relative to the flicker plus white noise models are shown in Table 1. The values shown indicate the improvement of the fit of the noise model to the data. A positive number indicates that model fits better than the flicker plus white noise model. (All noise models have a white noise component; I may forget to state it explicitly). A negative number indicates a worse fit of that model relative to the flicker model. The more positive the MLE value, the 'better' the noise model fits the data. In all cases, the flicker model is better than the random walk model. In some cases, the more general power-law model is significantly better than the flicker model. Also, the flicker plus band-pass filtered (BP1) usually provides a better fit than just flicker. When band-pass filtered noise is added to random walk, it usually improves the fit relative to the random-walk only model and, for many sites, it is not much worse than the flicker only model. I would judge a change of MLE less than 2 or 3 not to be significant. (In principle, one can compute confidence intervals of the improvement, but that takes many simulations of noisy data.)

Another test whether any or all of these noise models are consistent with the data is to evaluate the spectrum of wander (Agnew, 1992 *GRL*) for each time-series and test that spectrum against the ranges of wander derived from a series of simulated data having the same noise model as the real data. Wander, $w(\tau)$ is defined as function of period τ as:

$$w^2(\tau) = \frac{1}{T}\int (r(t+\tau) - r(t))^2 dt$$

and where T is the length of the time series and where r(t) is the time-series data residual after the average value, rate, and annual periodicity have been removed from the observed. For each combination of time-series and model, I evaluated this function numerically. Figure 3 shows a case for the east component of DRAO. In addition to estimating wander for the data residual, confidence limits for rejecting a candidate model can be determined by simulation. For instance, for a random walk model, 100 sets of simulated data are made using the amplitude of random walk (and white) noise estimated from the real data. For each set, a wander spectra is computed. Then, at each period, the values of wander from the 100 simulations are sorted from largest to smallest. From these lists of sorted numbers, the 68% and 95% confidence values are identified. In addition, a mean and standard deviation is derived. At each period, the value of wander for the real data is subtracted from the average from the simulated data and normalized by the standard deviation of the simulated data. For all periods, this statistic is squared and summed to form a χ^2 statistic. The value of χ^2 is evaluated in terms of a rejection confidence. These rejection confidences are shown in Table 2. In almost all the cases, the random-walk model is rejected.

Because the χ^2 statistic maybe too severe rejecting models, I also performed a visual inspection of the wander spectra from each site and model. I found in many cases where χ^2 indicates that all of the noise models should be rejected, the actual inspection of spectra indicate that some models do mimic much of the real data. This is illustrated in Figure 4 for the east component of CAB1. In fact, the wander spectra have large

fluctuations at periods less than 1-month that are not accounted for by any of the noise models. However, the long-period spectra seems well represented by all of the noise models. Part of the explanation for these short period variations is, according to Ken Hurst, due to improper modeling of the ocean loading tide for coastal sites. One of the beat frequencies for the Earth-tide has a period of 13.65 days. When a new set of noise models are estimated for CABL with an additional periodicity of 13.65 days, these models fit the observations better than the models without the 13.65 day period. (The amplitude of the 13.65 day period is 0.6 mm). This improvement is shown in Figure 5 where it is noted that the short period fluctuations of wander have decreased. It is likely that the ocean loading tide still contaminates the real data. In processing the phase data into a single position for each day, it is likely that the un-modeled tidal-components become aliased.

Although general power-law noise is an attractive model since is seems to model the noise character best, I prefer either the flicker noise or random-walk plus band-pass filtered noise models. From the visual inspections, both of these models appear attractive. The flicker noise alternative to power-law noise is attractive because it is simpler (index equals 1) and, if one averages the indices found for the power-law model, that average is only slightly less than 1. The equivalent functions of the power density for the power-law model is shown in Figure 6. Clearly, none of the sites are random-walk. Most of the slopes of the low frequency components are less than 1 with several close to 0.5 when these components are not too different that purely white noise (slope of 0). In fact, with the short time spans of many of the data, it is difficult to unambiguously resolve the temporally correlated part of the noise spectra. This is especially problematic since for many of the spectra, the annual term dominates the noise and this could leak into nearby frequencies. Hence, for simplicity, this suggests that flicker noise provides an adequate noise model.

An attractive alternative (at least to me) is a combination of random-walk plus band-pass filtered noise. These spectra are illustrated in Figure 7. At the longest periods, the spectra are forced to be random walk which, I believe, is due to random monument motions. At periods around 1 year, the spectra is peaked but smeared over several frequency bands. If one were to fit a linear trend over the periods representing band-pass of the filter, a flicker noise character might be indicated. This relation most apparent for the two IGS stations which are the longest time-series analyzed here. The explanation of the broad-band, seasonal noise is probably a combination of a season wobble of the monument and biases or systematic errors in the GPS processing.

Since the MLE method is computationally intense, (for the IGS sites with 7 years of data, it takes about 8-10 minutes to invert the covariance matrix; given the MLE routine tries nearly 200 different combination of parameters, it takes about 1-day to compute the noise parameters for one noise model for one time-series!) I explored a simpler method to estimate the noise components. Assuming that the time-series does not have significant gaps or offsets, standard power spectral techniques can be used to estimate the size of the flicker (or random walk) and white noise components. GPS data often satisfy these criteria of short, infrequent data gaps, and offsets that are easily removed. To deal with the data gaps that exist, these can be filled with interpolated values. I use linear interpolation but, to these interpolates, I add white noise. I determine the white noise from the data by removing a running mean consisting of 2 to 3 days length. The white noise is determined from the residuals of that running mean. From the data set with its gaps filled, a power spectra is computed using standard FFTs. For the results shown in Figure 8, I have not done any smoothing; rather, the spectra can be considered a periodogram. I fit to the raw spectral values a curve representing a combination of flicker and white noise.

Because the longest periods of the spectrum are poorly determined (They depend upon proper removal of a linear trend --- this trend is different depending upon whether the data are random-walk or white noise), I down-weight the long period components for curve fitting. Comparison of the amplitudes flicker and white noise that I get from spectral analysis indicate that the spectrally derived estimates for the flicker noise are within a factor of 2 of the MLE determined amplitudes. (The white noise is within 10%.) This method is probably the best way for most investigators to compute noise levels of their data.

Once the parameters for the data covariance are specified, the rates, offsets, and other parameters needed to model the deformation as a function of time can be estimated. Importantly, these parameters and their standard error are determined. Using the flicker and white noise models from the better GPS sites, the standard error in rate as a function of the length of the time-series is illustrated in Figure 2 and Table 4. Although I could not resolve any additional contribution due to random-walk noise, if present at the $0.5\text{mm}/\sqrt{\text{yr}}$ level, it does increase the uncertainty of the rate estimates. In addition, if seasonal variations are modeled as a single sine wave, that additional unknown affects the rate uncertainty for time-spans of less than one year. This is illustrated in Figure 9.

One of the goals of this paper was to try to detect whether monument noise might be present in some of the GPS time-series, especially from the data with the longest time span (the IGS sites) or from the Coast Guard sites with antennas mounted on potentially wobbly towers. However, rather than finding any random-walk (or high index power-law) models for these data, I see that the flicker amplitudes are correlated with the white noise amplitudes (Figure 1). If monument noise was present and causing the 1/f relation of flicker noise, I would not have expected a strong correlation between flicker amplitude and white noise. The results shown in Figure 1 indicate that the flicker amplitude is about 40% of the white noise amplitude. With more GPS data available, this correlation should be testable.

The other possible measure of monument noise is the seasonal amplitude. From the experience of Langbein and Johnson [1997], a large seasonal amplitude is indicative of a poor monument, but a low seasonal amplitude does not indicate that the monument is good. The estimates of seasonal noise is provided in Table 4. Unfortunately, GPS processing may introduce systematic biases that could manifest itself as seasonal noise. Since the two Coast Guard sites don't have significantly greater amounts of seasonal variation than the other sites, it is not possible to state that monument noise is the sole cause to seasonal variation.

Conclusions:

1 Flicker plus white noise provides an adequate characterization of noise in GPS data. We can reject the purely random walk model. Random-walk plus band-pass filtered noise might be a suitable model but we'll need longer time-series to be able to favor either the flicker (or power law) or the random-walk plus band-pass filtered model.

2 From this set of GPS data, it appears that the flicker component is about 40% of the white noise component. This suggests that the correlated part of the noise is due to instrumentation issues related to the hardware, ie. the antenna, or to the software (inadequate models in the GPS software).

3 Even though random-walk noise is not detectable in these time-series, a low-level amounts of this noise can make a significant contribution to the standard error in rate for periods in excess of a few months.

4 Given the large amount of GPS data that will be available soon, the MLE technique is too time consuming to provide noise estimates routinely. Rather, if the GPS data do not have too many gaps and none of the gaps are too long, standard power spectra estimation can provide reasonable estimates of noise. MLE technique should be used with data with significant gaps or to define generic noise models needed to characterize the error spectra of GPS.

Table 1

Change in MLE relative to FL model **East**

	PL	BP1_FL	RW	BP1_RW
cabl	4.59	-0.00	-10.29	-7.06
cme1	0.53	4.58	-5.34	4.58
fts1	0.47	0.01	-11.00	-5.12
pabh	0.38	2.74	-5.57	2.74
redm	0.43	0.00	-1.20	-0.97
albh	0.64	1.62	-12.27	-1.18
drao	0.16	0.29	-9.61	-2.24

Change in MLE relative to FL model **North**

	PL	BP1_FL	RW	BP1_RW
cabl	0.14	0.00	-12.76	-3.21
cme1	1.24	0.00	-14.50	-3.17
fts1	0.28	0.42	-9.75	-3.62
pabh	0.04	1.62	-2.77	1.60
redm	0.20	4.05	-3.18	4.05
albh	0.91	0.00	-14.02	-4.43
drao	0.01	0.00	-11.81	-6.38

Change in MLE relative to FL model **Up**

	PL	BP1_FL	RW	BP1_RW
cabl	0.05	-0.00	-4.37	-3.69
cme1	0.03	0.03	-8.45	-3.56
fts1	0.49	0.00	-3.64	-2.61
pabh	6.50	-0.43	-6.71	-0.44
redm	4.06	1.44	0.00	1.44
albh	0.15	0.01	-23.22	-12.83
drao	1.56	-0.00	-29.78	-18.51

Table 2

Rejection confidence: **East**

	Noise Model type				
	RW	FL	RW+BP1	FL+BP1	PL
albh	**100**	74	**98**	88	74
drao	**100**	1	**91**	1	0
cabl	**100**	**100**	**100**	**100**	**100**
cabl-13.65	**100**	**100**	**100**	**96**	85
pabh	**100**	**100**	**100**	**100**	**100**
redm	1	25	11	17	14
cme1	**100**	**98**	**100**	**98**	80
fts1	**100**	87	**95**	**100**	1

Rejection confidence: **North**

	Noise Model type				
	RW	FL	RW+BP1	FL+BP1	PL
albh	**100**	16	86	49	4
drao	**99**	7	17	4	1
cabl	**100**	0	16	0	0
cabl-13.65	**100**	0	6	0	0
pabh	58	74	85	69	66
redm	**94**	**100**	**100**	**100**	**91**
cme1	**100**	62	**100**	92	**99**
fts1	**100**	**100**	**100**	**100**	**100**

Rejection confidence: **UP**

	Noise Model type				
	RW	FL	RW+BP1	FL+BP1	PL
albh	**100**	**100**	**100**	**97**	**100**
drao	**100**	79	**100**	**91**	69
cabl	**100**	**91**	**100**	**99**	**92**
cabl-13.65	80	**100**	**97**	**97**	19
pabh	**100**	**96**	**99**	**99**	82
redm	25	16	20	7	0
cme1	**100**	3	48	5	4
fts1	**100**	**99**	**100**	**100**	**100**

Total number rejected $P > 90$

	Noise Model type				
	RW	FL	RW+BP1	FL+BP1	PL
East	6	3	6	4	1
North	6	2	3	3	3
Up	5	4	5	5	2
All	17	9	14	12	6

Table 3

Rejection confidence *visual*: **EAST**

	Noise Model type				
	RW	FL	RW+BP1	FL+BP1	PL
albh	y	n	n	n	n
drao	y	n	n	n	n
cabl					
cabl-13.65	y	n	y	n	n
pabh	n	n	n	n	n
redm	n	n	n	n	n
cme1	y	n	n	n	n
fts1	y	n	n	n	n

Rejection confidence *visual:* **North**

	Noise Model type				
	RW	FL	RW+BP1	FL+BP1	PL
albh	y	n	n	n	n
drao	y	n	n	n	n
cabl	y	n	n	n	n
cabl-13.65	y	n	n	n	n
pabh	n	n	n	n	n
redm	n	n	n	n	n
cme1	n	n	n	n	n
fts1	y	n	n	n	n

Rejection confidence *visual*: **UP**

	Noise Model type				
	RW	FL	RW+BP1	FL+BP1	PL
albh	y	n	n	n	n
drao	y	n	n	n	n
cabl	n	n	n	n	n
cabl-13.65	n	n	n	n	n
pabh	n	n	n	n	n
redm	n	n	n	n	n
cme1	y	n	n	n	n
fts1	n	n	n	n	n

Total number rejected *visually*

	Noise Model type				
	RW	FL	RW+BP1	FL+BP1	PL
East	5	0	1	0	0
North	4	0	0	0	0
Up	3	0	0	0	0
All	12	0	1	0	0

Table 4

Flicker plus white noise amplitudes: **EAST**

	Flicker	White	Seasonal	13.65-day
albh	0.884	1.983	0.422	
drao	0.654	2.115	0.608	
cabl	0.894	2.014	1.127	
cabl-13.65	0.763	2.037	1.118	0.6
pabh	0.542	1.824	0.676	
redm	0.675	2.461	0.875	
cme1	1.167	4.326	0.732	
fts1	1.530	2.596	0.879	

Flicker plus white noise amplitudes: **NORTH**

	Flicker	White	Seasonal	13.65-day
albh	0.476	1.040	0.174	
drao	0.484	1.200	0.368	
cabl	0.545	1.063	0.552	
cabl-13.65	0.530	1.062	0.552	0.2
pabh	0.309	1.005	0.344	
redm	0.594	1.242	1.034	
cme1	1.088	2.221	2.067	
fts1	0.825	1.503	0.971	

Flicker plus white noise amplitudes: **UP**

	Flicker	White	Seasonal	13.65-day
albh	1.919	3.368	1.504	
drao	1.781	3.649	2.130	
cabl	1.608	3.363	1.431	
cabl-13.65	1.520	3.361	1.421	0.9
pabh	1.085	3.282	1.201	
redm	0.006	4.667	0.842	
cme1	3.144	6.343	3.053	
fts1	1.900	4.497	2.283	

Figure 1: Scatter plot of estimated values of white noise versus that for flicker noise using 7 sites described in the paper. Linear trend shows the high correlation between white and flicker noise; the flicker noise component is about 40% of the white noise. Only one point deviates grossly from this relation. That point is for the vertical component of REDM where high white noise precludes the detection of temporally correlated noise due to its short (2 year) time span.

Figure 2: Estimates of standard errors in secular rate for a variety of time-spans and noise models. The 3, dark lines are error estimates with different combination of white and flicker noise; the bottom trace is 1.0 mm white and 0.4 mm flicker, the middle trace is 2.0 mm white and 0.8 mm flicker, and the top trace is 3.5 mm white and 1.4 mm flicker. These three models are generally noise amplitudes for the best sites for north, east, and up respectively. The colored curves shows the influence of random-walk has upon the above model. The red curve is an additional $0.5\text{mm}/\sqrt{\text{yr}}$ random-walk noise, the blue is $1.0\text{mm}/\sqrt{\text{yr}}$, and green is $2.0\text{mm}/\sqrt{\text{yr}}$.

Figure 3: Plot of wander spectra for the east component of DRAO against wander estimated from simulated data having similar noise as estimate from the real data. The heavy line is wander from the real data and the lighter lines represent confidence bounds based upon 100 simulation of the data. The dashed lines are the 68% confidence limits, the outer light, solid lines are the 95% confidence limits, and the middle, light line is the average wander from the simulated data. Also shown are the noise components used to simulate the data. Confidence levels for rejecting the candidate model are also shown; one for the entire wander spectra, and a second value for the wander spectra at the longer periods, $\tau > 30 - \text{days}$.

Figure 4: As as Figure 3 but for the east component of CABL

Figure 5: As as Figure 4 for the east component of CABL but with 0.6 mm of 13.65 period sinusoid removed from the data. This period is probably due to improper removal of the ocean load component of the Earth Tide. It seems to affect east and up more than the north component.

Figure 6: Equivalent power spectra density derived from a power-law plus white noise model estimated using MLE. Each figure shows one component, east, north, and up. Reference power densities for various amplitudes of random walk noise are shown.

Figure 7: Equivalent power spectra density derived from a random-walk and band-pass filtered noise plus white noise model estimated using MLE. Each figure shows one component, east, north, and up. Reference power densities for various amplitudes of random walk noise are shown.

Figure 8: The periodogram of east component from ALBH is shown with a thin dark line. Note the spike at 13.65 days. The blue curve is the equivalent PSD function using the MLE technique. The solid, red line is the PSD function using the periodogram to estimate the size of the flicker and white noise components. The dashed, red line is the PSD function for flicker and white noise estimated from the periodogram but constraining the value of white noise. This is described in the text; it is the RMS scatter of residuals after removing a running mean from the data. For estimating the parameters of the red curves, the components of longest periods in the periodogram have been down-weighted.

Figure 9: Same as Figure 2 but with the additional parameters of a 365 day sinusoid added to the deformation model with time.

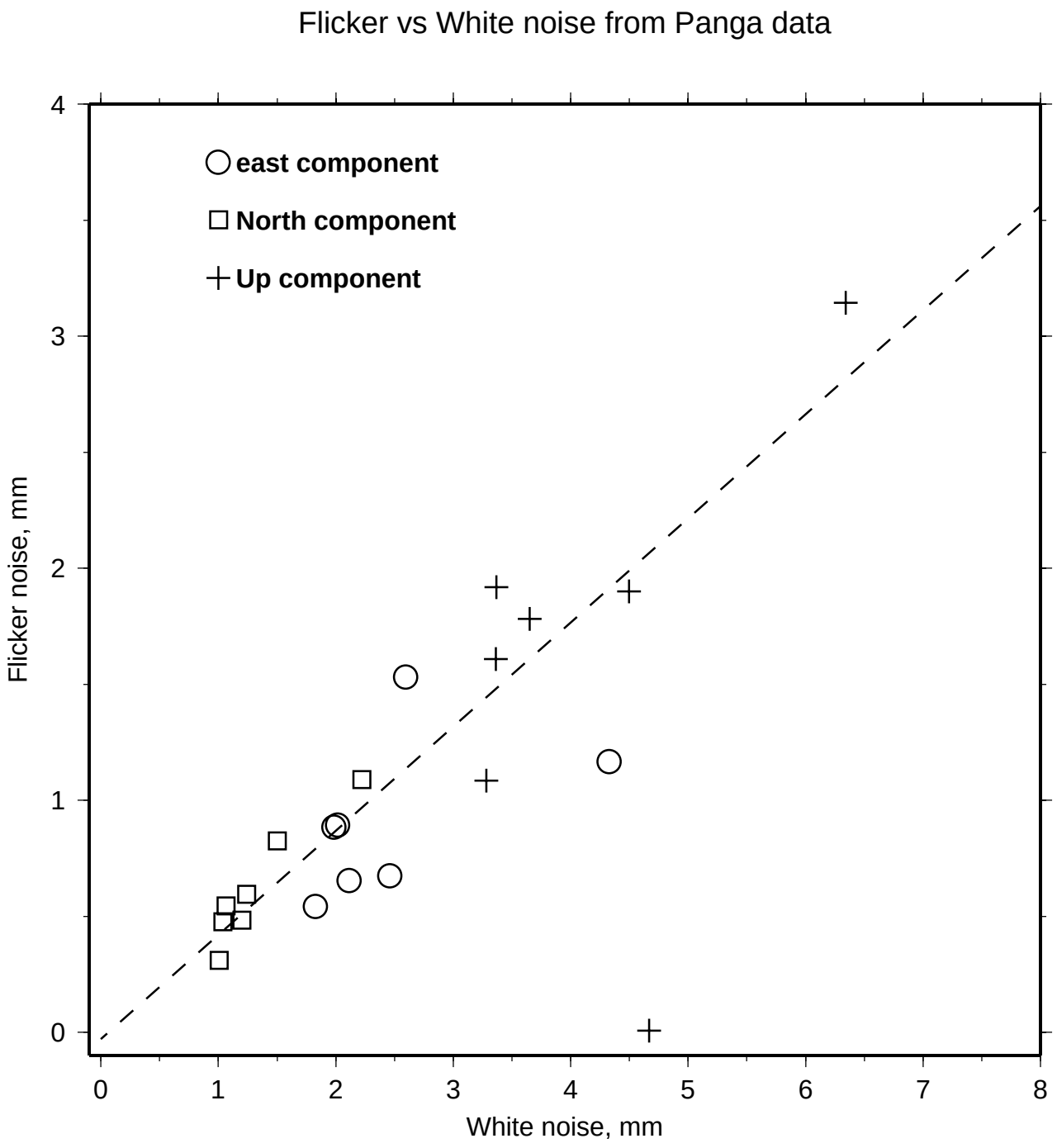
Flicker vs White noise from Panga data
east component
North component
Up component
Flicker noise, mm
White noise, mm
0
1
2
3
4
5
6
7
8

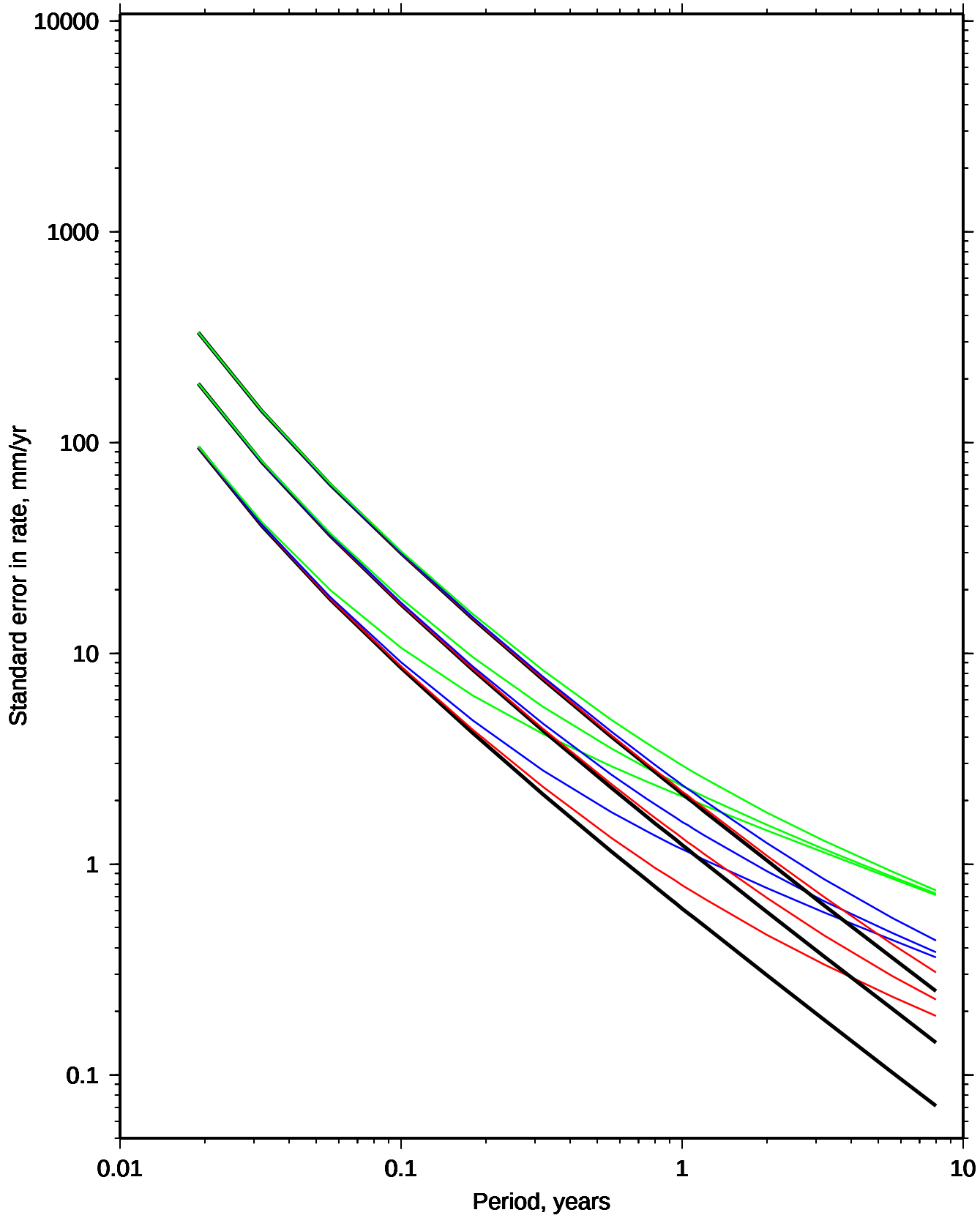
10000
1000
100
10
1
0.1
Standard error in rate, mm/yr
0.01
0.1
1
10
Period, years

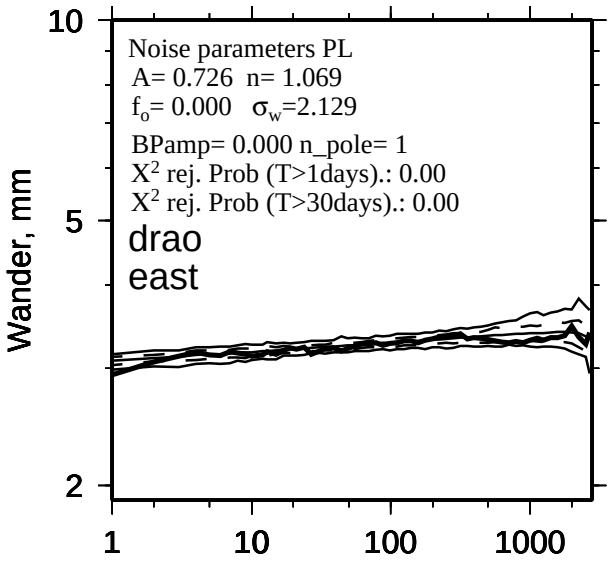
Noise parameters PL
A= 0.726 n= 1.069
f_o= 0.000 σ_w=2.129
BPamp= 0.000 n_pole= 1
X^2 rej. Prob (T>1days).: 0.00
X^2 rej. Prob (T>30days).: 0.00
drao
east
Wander, mm
10
5
2
1
10
100
1000

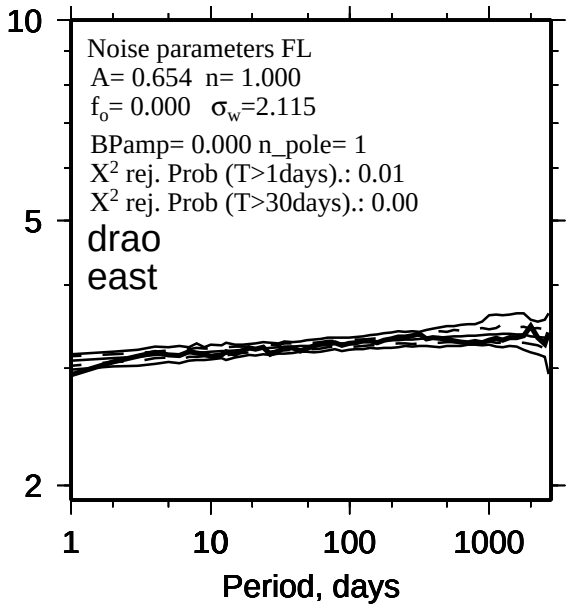
Noise parameters FL
A= 0.654 n= 1.000
f_o= 0.000 σ_w=2.115
BPamp= 0.000 n_pole= 1
X^2 rej. Prob (T>1days).: 0.01
X^2 rej. Prob (T>30days).: 0.00
drao
east
10
5
2
1
10
100
1000
Period, days

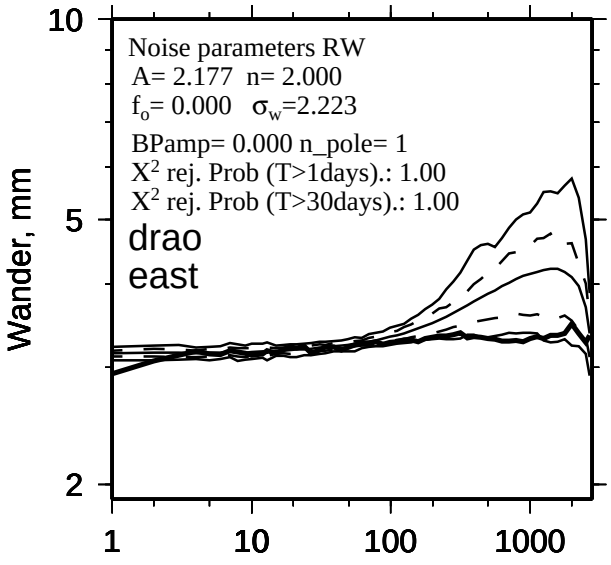
Noise parameters RW
A= 2.177 n= 2.000
f_o= 0.000 σ_w=2.223
BPamp= 0.000 n_pole= 1
X^2 rej. Prob (T>1days).: 1.00
X^2 rej. Prob (T>30days).: 1.00
drao
east
Wander, mm
10
5
2
1
10
100
1000

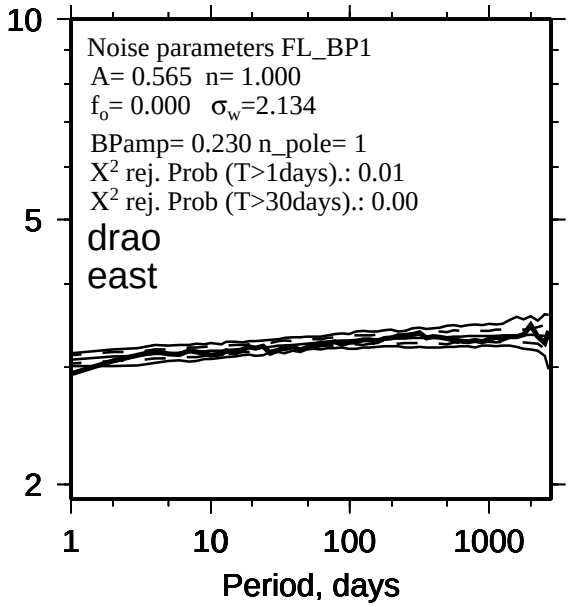
Noise parameters FL_BP1
A= 0.565 n= 1.000
f_o= 0.000 σ_w=2.134
BPamp= 0.230 n_pole= 1
X^2 rej. Prob (T>1days).: 0.01
X^2 rej. Prob (T>30days).: 0.00
drao
east
10
5
2
1
10
100
1000
Period, days

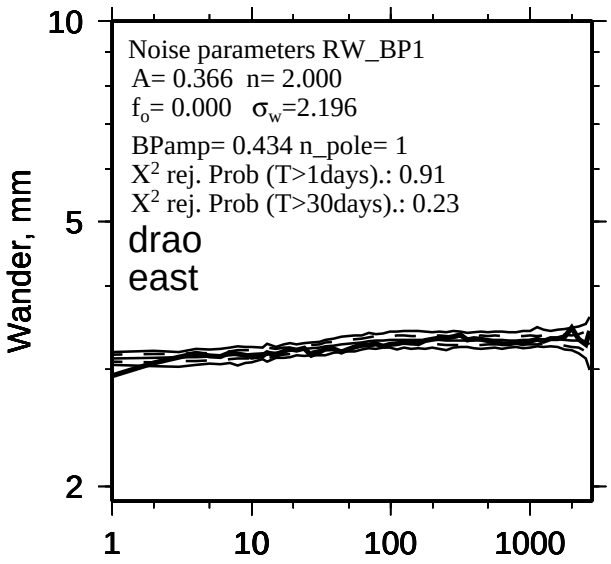
Noise parameters RW_BP1
A= 0.366 n= 2.000
f_o= 0.000 σ_w=2.196
BPamp= 0.434 n_pole= 1
X^2 rej. Prob (T>1days).: 0.91
X^2 rej. Prob (T>30days).: 0.23
drao
east
Wander, mm
10
5
2
1
10
100
1000

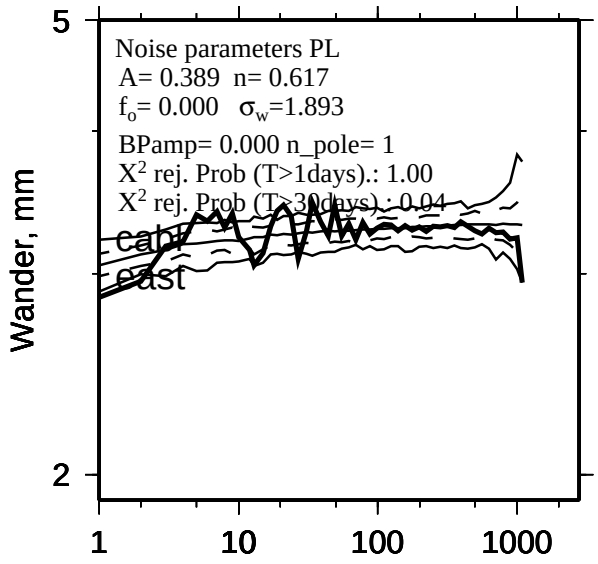
Noise parameters PL
A= 0.389 n= 0.617
f_o= 0.000 σ_w=1.893
BPamp= 0.000 n_pole= 1
X^2 rej. Prob (T>1days).: 1.00
X^2 rej. Prob (T>30days).: 0.04
cabl
east
Wander, mm
5
2
1
10
100
1000

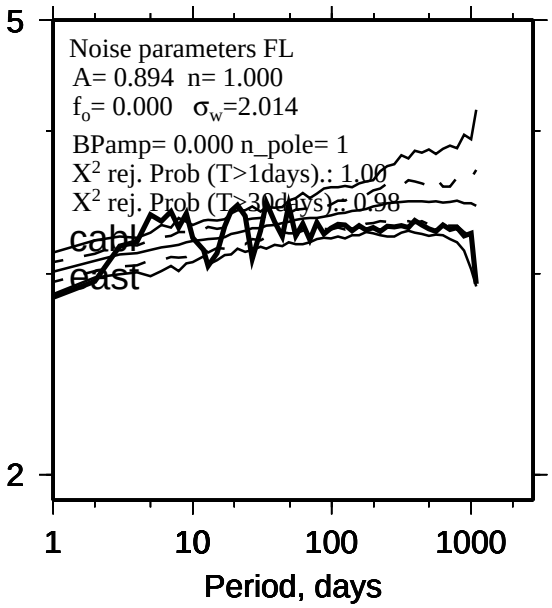
Noise parameters FL
A= 0.894 n= 1.000
f_o= 0.000 σ_w=2.014
BPamp= 0.000 n_pole= 1
X^2 rej. Prob (T>1days).: 1.00
X^2 rej. Prob (T>30days).: 0.98
cabl
east
5
2
1
10
100
1000
Period, days

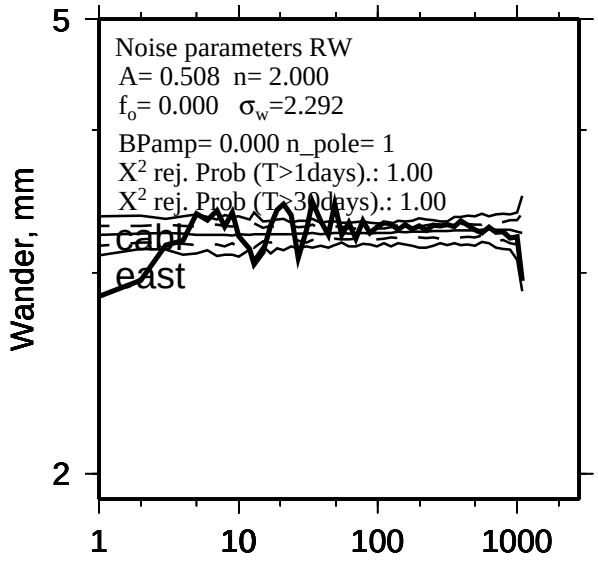
Noise parameters RW
A= 0.508 n= 2.000
f_o= 0.000 σ_w=2.292
BPamp= 0.000 n_pole= 1
X^2 rej. Prob (T>1days).: 1.00
X^2 rej. Prob (T>30days).: 1.00
cabl
east
Wander, mm
5
2
1
10
100
1000

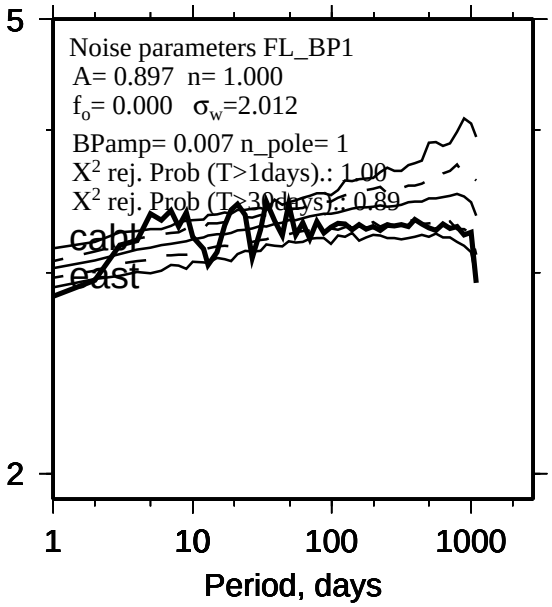
Noise parameters FL_BP1
A= 0.897 n= 1.000
f_o= 0.000 σ_w=2.012
BPamp= 0.007 n_pole= 1
X^2 rej. Prob (T>1days).: 1.00
X^2 rej. Prob (T>30days).: 0.89
cabl
east
5
2
1
10
100
1000
Period, days

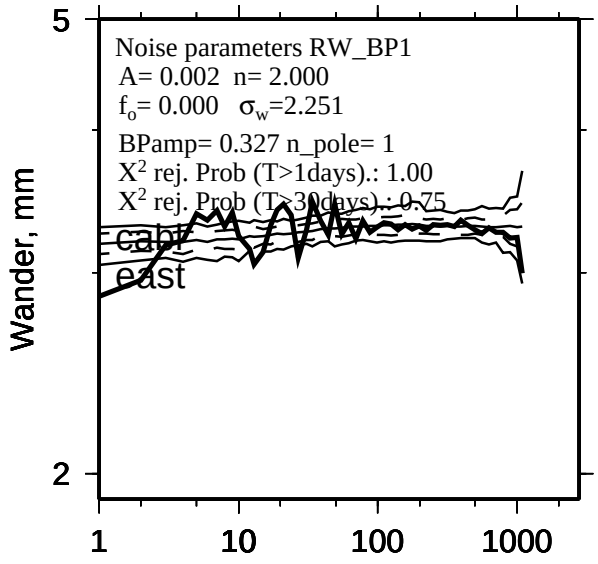
Noise parameters RW_BP1
A= 0.002 n= 2.000
f_o= 0.000 σ_w=2.251
BPamp= 0.327 n_pole= 1
X^2 rej. Prob (T>1days).: 1.00
X^2 rej. Prob (T>30days).: 0.75
cabl
east
Wander, mm
5
2
1
10
100
1000

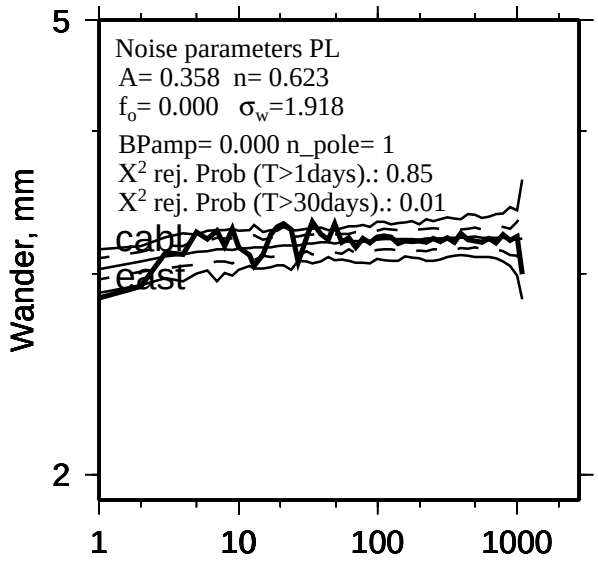
Noise parameters PL
A= 0.358 n= 0.623
f_o= 0.000 σ_w=1.918
BPamp= 0.000 n_pole= 1
X^2 rej. Prob (T>1days).: 0.85
X^2 rej. Prob (T>30days).: 0.01
cabl
east
Wander, mm
5
2
1
10
100
1000

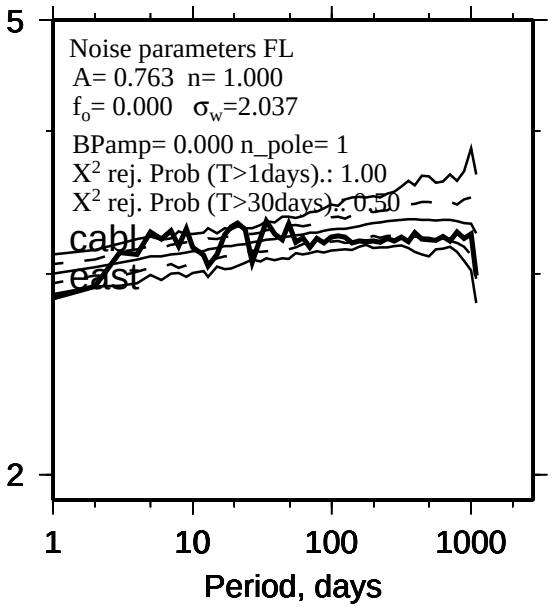
Noise parameters FL
A= 0.763 n= 1.000
f_o= 0.000 σ_w=2.037
BPamp= 0.000 n_pole= 1
X^2 rej. Prob (T>1days).: 1.00
X^2 rej. Prob (T>30days).: 0.50
cabl
east
5
2
1
10
100
1000
Period, days

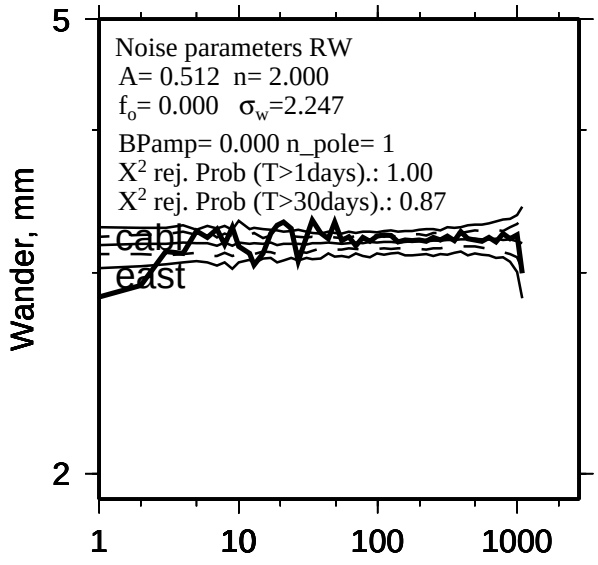
Noise parameters RW
A= 0.512 n= 2.000
f_o= 0.000 σ_w=2.247
BPamp= 0.000 n_pole= 1
X^2 rej. Prob (T>1days).: 1.00
X^2 rej. Prob (T>30days).: 0.87
cabl
east
Wander, mm
5
2
1
10
100
1000

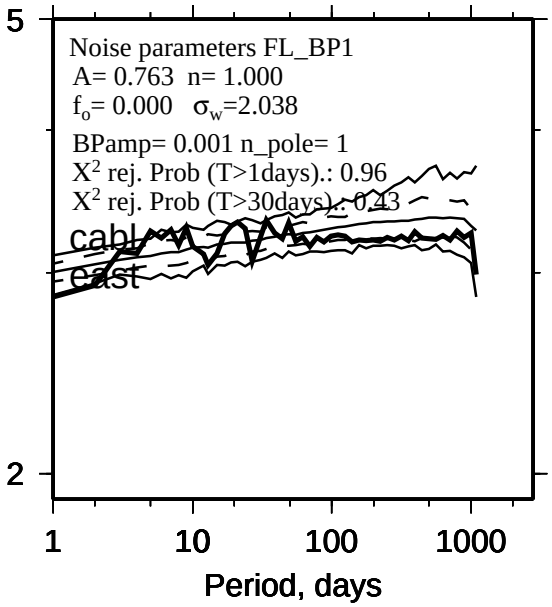
Noise parameters FL_BP1
A= 0.763 n= 1.000
f_o= 0.000 σ_w=2.038
BPamp= 0.001 n_pole= 1
X^2 rej. Prob (T>1days).: 0.96
X^2 rej. Prob (T>30days).: 0.43
cabl
east
5
2
1
10
100
1000
Period, days

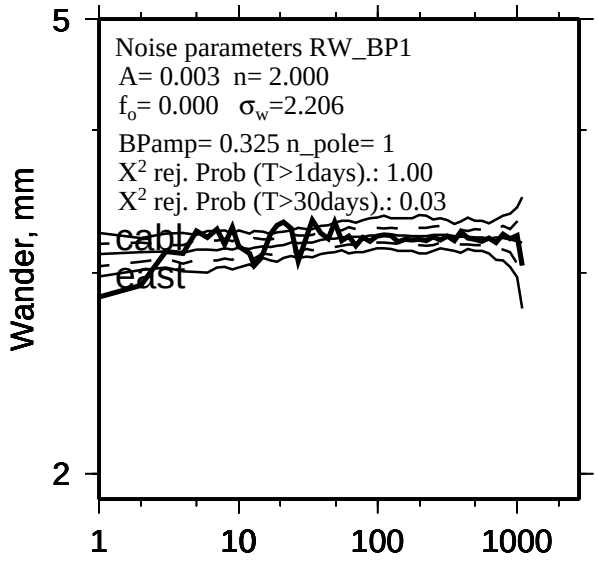
Noise parameters RW_BP1
A= 0.003 n= 2.000
f_o= 0.000 σ_w=2.206
BPamp= 0.325 n_pole= 1
X^2 rej. Prob (T>1days).: 1.00
X^2 rej. Prob (T>30days).: 0.03
cabl
east
Wander, mm
5
2
1
10
100
1000

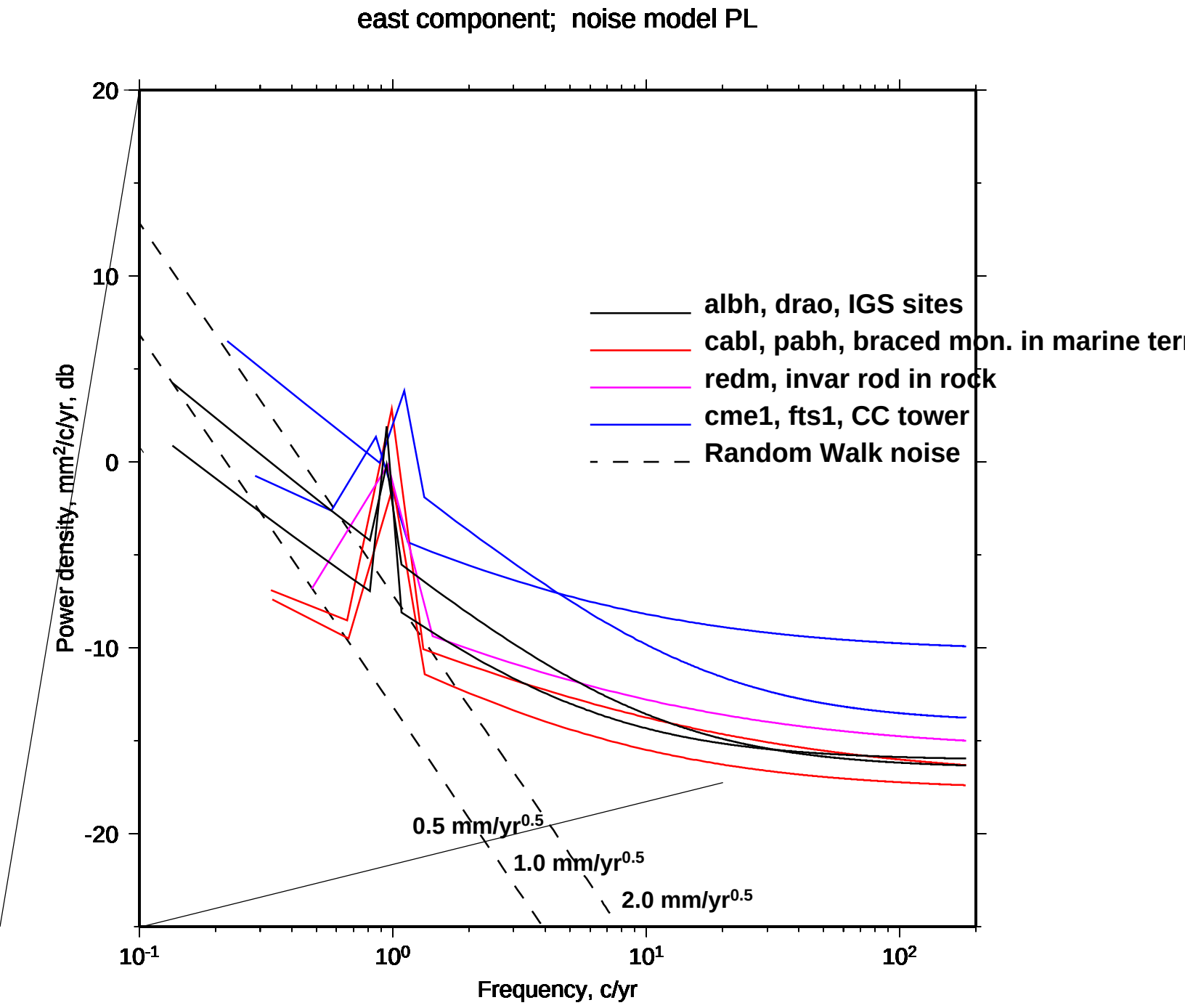
east component; noise model PL
20
10
0
-10
-20
Power density, mm²/c/yr, db
10⁻¹
10⁰
10¹
10²
Frequency, c/yr
albh, drao, IGS sites
cabl, pabh, braced mon. in marine ter
redm, invar rod in rock
cme1, fts1, CC tower
Random Walk noise
0.5 mm/yr^0.5
1.0 mm/yr^0.5
2.0 mm/yr^0.5

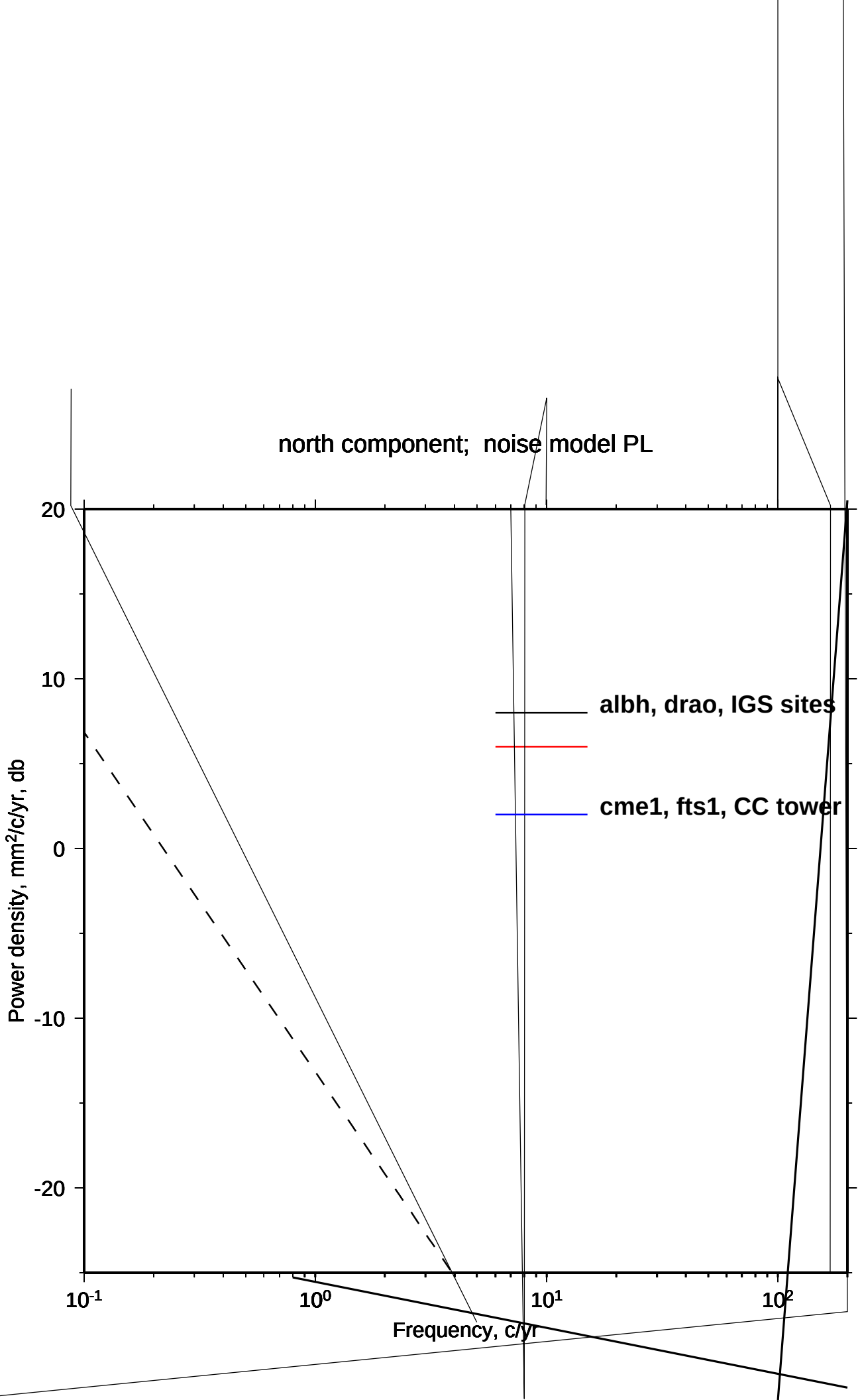
north component; noise model PL
20
10
0
-10
-20
Power density, mm²/c/yr, db
albh, drao, IGS sites
cme1, fts1, CC tower
10⁻¹
10⁰
10¹
10²
Frequency, c/yr

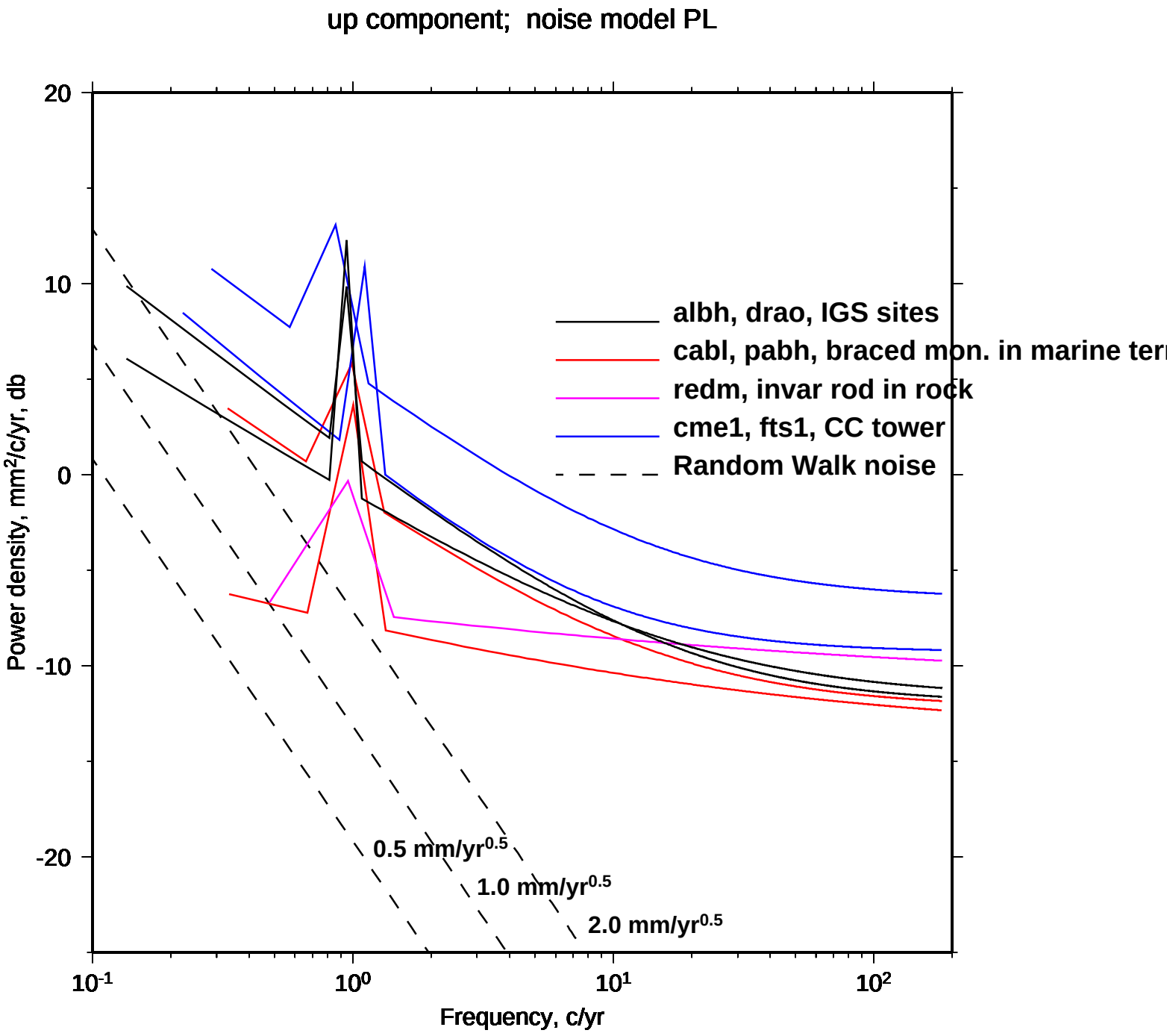
up component; noise model PL
20
10
0
-10
-20
Power density, mm²/c/yr, db
10⁻¹
10⁰
10¹
10²
Frequency, c/yr
albh, drao, IGS sites
cabl, pabh, braced mon. in marine ter
redm, invar rod in rock
cme1, fts1, CC tower
Random Walk noise
0.5 mm/yr^0.5
1.0 mm/yr^0.5
2.0 mm/yr^0.5

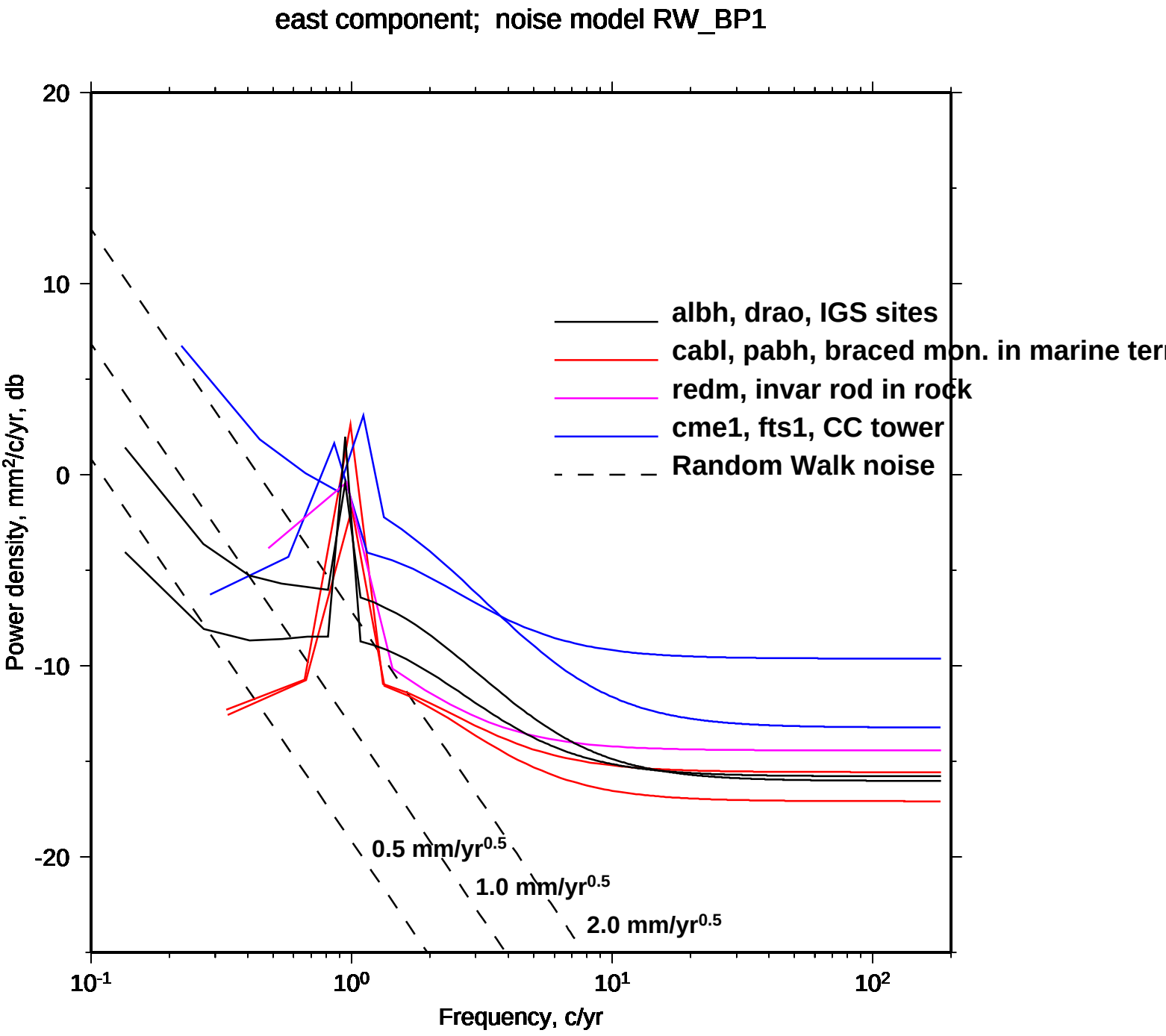
east component; noise model RW_BP1
20
10
0
-10
-20
Power density, mm²/c/yr, db
10⁻¹
10⁰
10¹
10²
Frequency, c/yr
albh, drao, IGS sites
cabl, pabh, braced mon. in marine ter
redm, invar rod in rock
cme1, fts1, CC tower
Random Walk noise
0.5 mm/yr^0.5
1.0 mm/yr^0.5
2.0 mm/yr^0.5

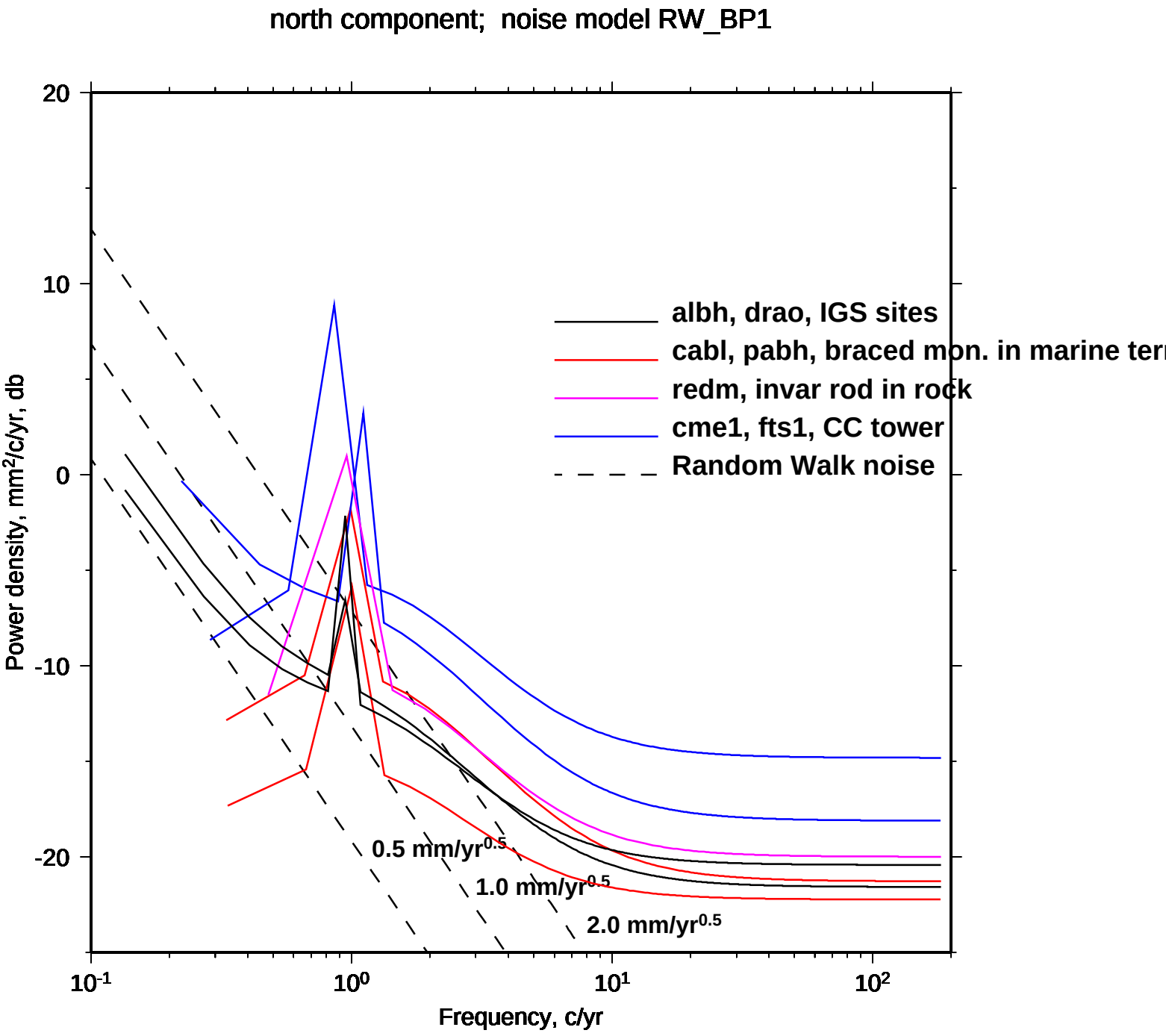
north component; noise model RW_BP1
20
10
0
-10
-20
Power density, mm²/c/yr, db
10⁻¹
10⁰
10¹
10²
Frequency, c/yr
albh, drao, IGS sites
cabl, pabh, braced mon. in marine ter
redm, invar rod in rock
cme1, fts1, CC tower
Random Walk noise
0.5 mm/yr^0.5
1.0 mm/yr^0.5
2.0 mm/yr^0.5

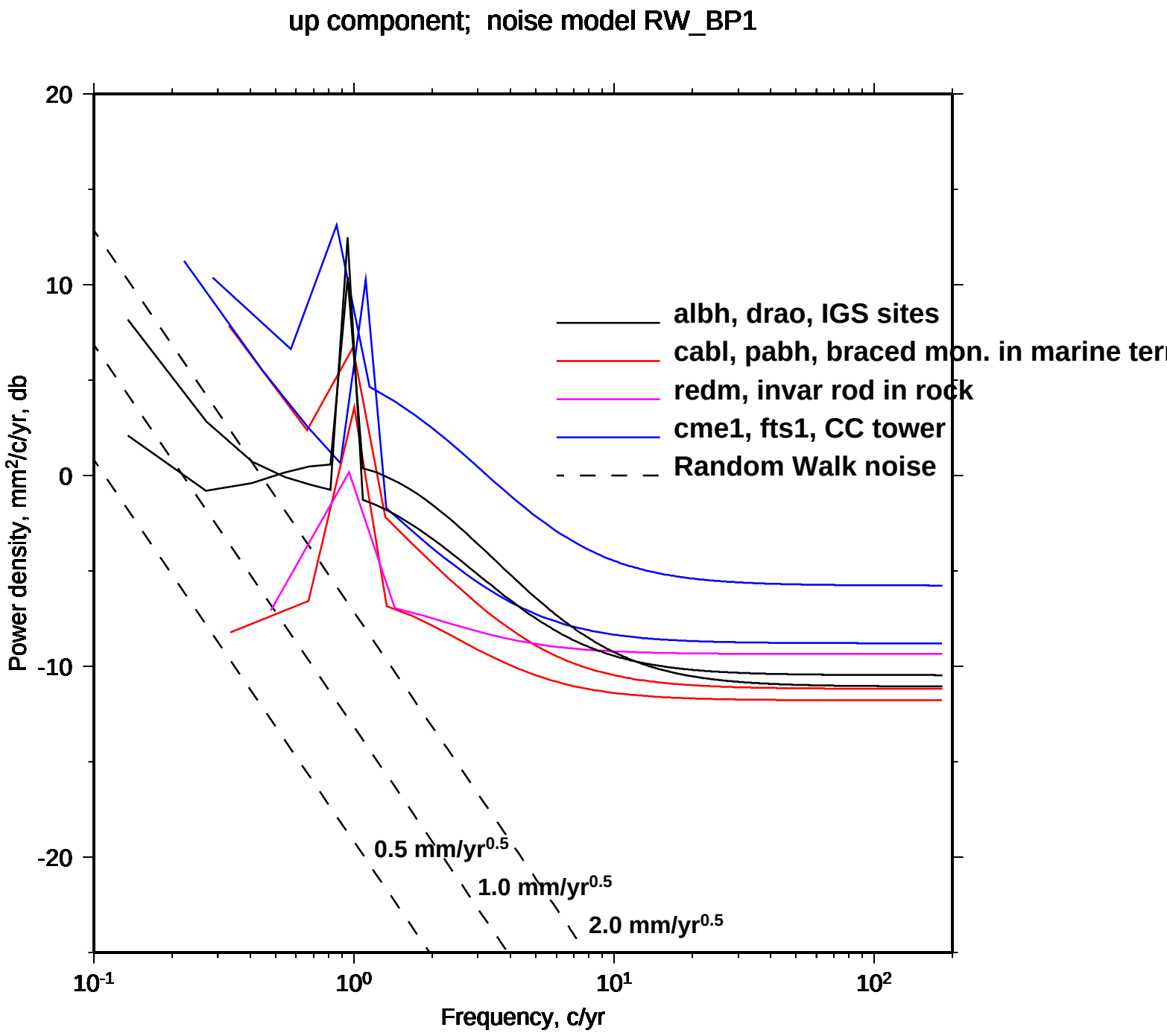
up component; noise model RW_BP1
20
10
0
-10
-20
Power density, mm²/c/yr, db
10⁻¹
10⁰
10¹
10²
Frequency, c/yr
albh, drao, IGS sites
cabl, pabh, braced mon. in marine ter
redm, invar rod in rock
cme1, fts1, CC tower
Random Walk noise
0.5 mm/yr^0.5
1.0 mm/yr^0.5
2.0 mm/yr^0.5

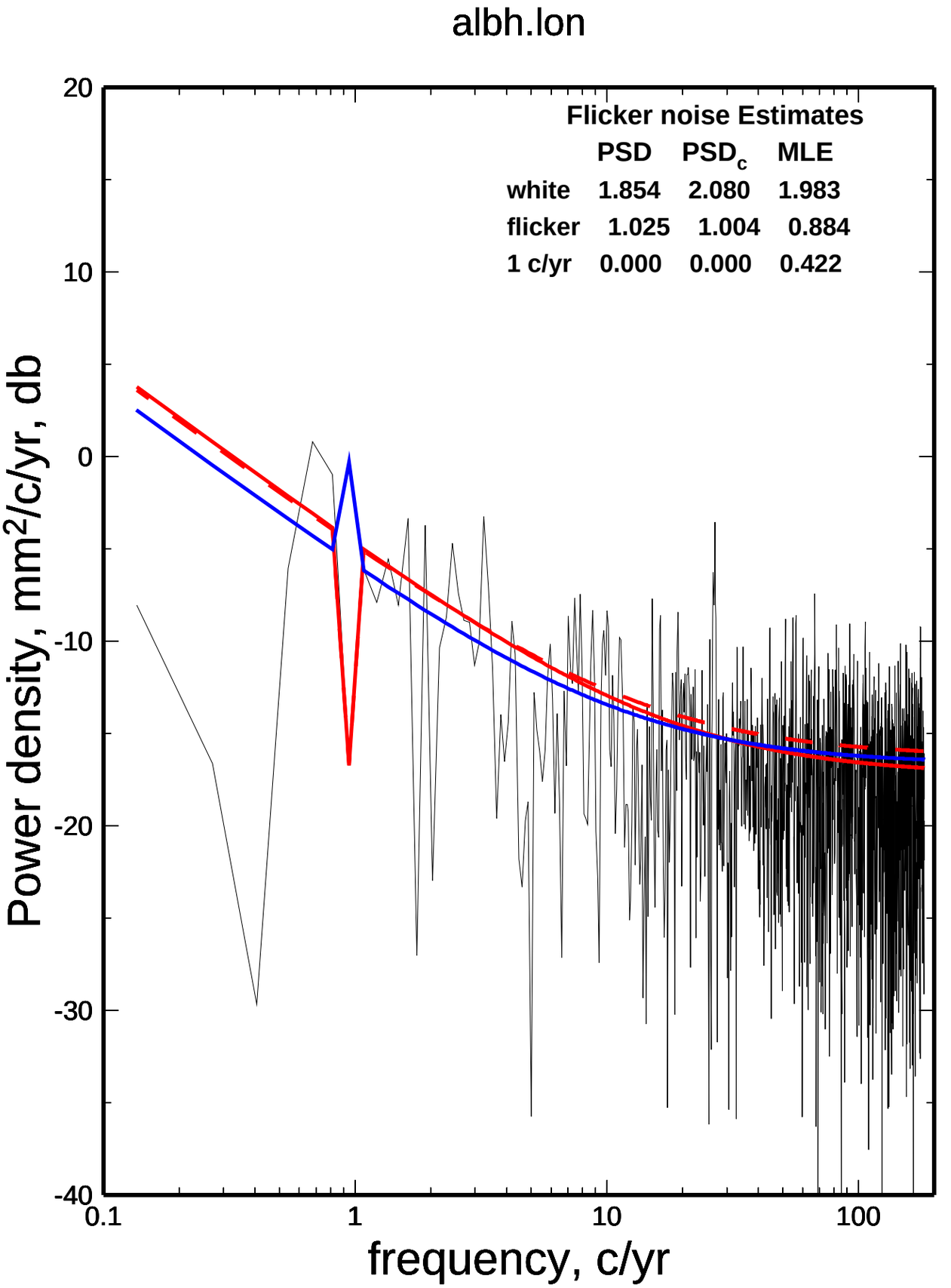
albh.lon
Flicker noise Estimates
PSD PSDc MLE
white 1.854 2.080 1.983
flicker 1.025 1.004 0.884
1 c/yr 0.000 0.000 0.422
Power density, mm²/c/yr, db
frequency, c/yr
20
10
0
-10
-20
-30
-40
0.1
1
10
100

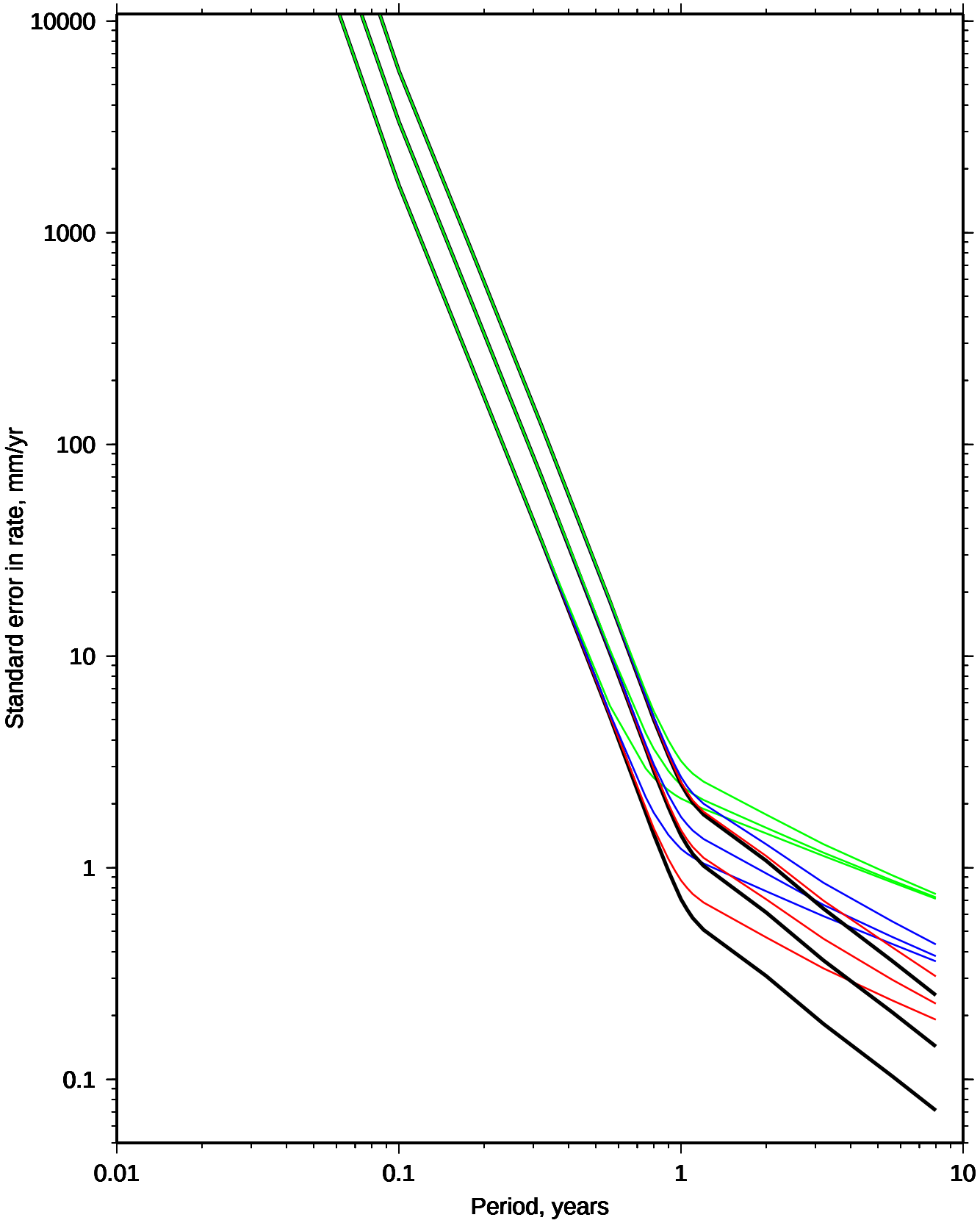
10000
1000
100
10
1
0.1
Standard error in rate, mm/yr
0.01
0.1
1
10
Period, years